PLASMA CHARACTERISATION OF
A DC CLOSED FIELD MAGNETRON SPUTTERING DEVICE

G. Serianni[a], V. Antoni[a,b], R. Cavazzana[a], G. Maggioni[c], E. Martines[a]
N. Pomaro[a], V. Rigato[c], M. Spolaore[a,b], L. Tramontin[a]

[a] *Consorzio RFX, Padova, Italy*
[b] *Istituto Nazionale Fisica della Materia — UdR Padova, Italy*
[c] *I.N.F.N. Laboratori Nazionali di Legnaro, Italy*

Magnetron sputtering deposition techniques are widely applied both in industrial processes and in advanced material development or treatment [1]. The working principle of these devices is the glow discharge between a cathode and the vacuum vessel. Below the cathode surface permanent magnets are located; in front of the cathode surface the magnetic field creates a zone ("magnetic trap") where the electron loss rate is reduced and the ionisation probability enhanced [2]. The ensuing ions, having Larmor radii much larger than the magnetic trap size, are accelerated by the electric field towards the cathode where they sputter particles which deposit as a film over a suitable substrate. The deposition process is strongly dependent on magnetic field and plasma parameters such as ion flux, plasma potential, electron temperature and density. The present work is dedicated to the characterisation, by means of Hall probes and cylindrical Langmuir probes, of a DC closed field unbalanced magnetron sputtering device for thin film deposition.

The vacuum chamber (length 1194 mm, height 755 mm, depth 734 mm) is equipped with two 250×140 mm^2 rectangular magnetron sources located in opposite positions (fig. 1); the distance between the source surfaces is 440 mm. They are negatively biased with respect to
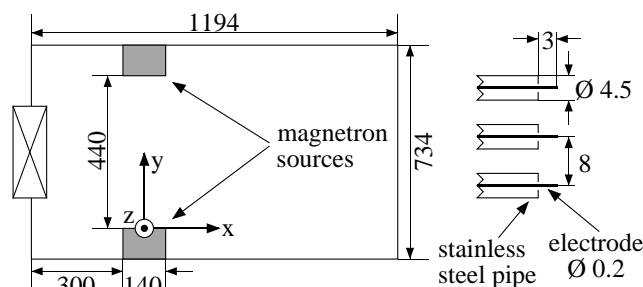
Fig. 1: Top view of the vacuum chamber (left). Scheme of the Langmuir probe system (right). Dimensions in mm.

the chamber walls by a DC current-controlled power supply. The delivered power can reach 20 kW. During the measurements presented herein the total power was 800 W and the total source current was 2 A. A power scan was also performed with applied power in the range 0.4 to 4 kW. The discharge gas was argon, the working pressure 0.1 Pa and the target material aluminium.

The magnetic field characterisation was obtained using Hall-effect sensors suitable for static fields and mounted on a mechanical supporting structure so as to simultaneously obtain all three components. Due to the position of the permanent magnets the expected magnetic field configuration is of the pole-opposed type, characterised by symmetries with respect to the (x,y), (y,z) and (x,z) planes (see fig. 1); z = 0 in the centre of the sources. Hence the magnetic field mapping was limited to the following two regions: $0 \le x \le 80$ mm and $0 \le y \le 210$ mm; $0 \le y \le 210$ mm and $0 \le z \le 90$ mm. The results of the magnetic measurements obtained in the horizontal plane (z = 0) are presented in fig. 2; the figure is split into two parts where different scales are used, since the absolute value of the magnetic field varies dramatically. As expected the magnetic field configuration is of the unbalanced type. The magnetic trap, defined as the region where the magnetic field lines intersect a cathode surface at both ends, is about 40 mm wide along x and extends up to 30 mm from the

cathode along y. It should be noticed that some magnetic field lines connect one cathode to the other. Also electrons confined in this area can contribute to ionisation; thus this region has specific features with respect to the outer one, as shown in the following.

The Langmuir probe system used in the present campaign is sketched on the right hand side
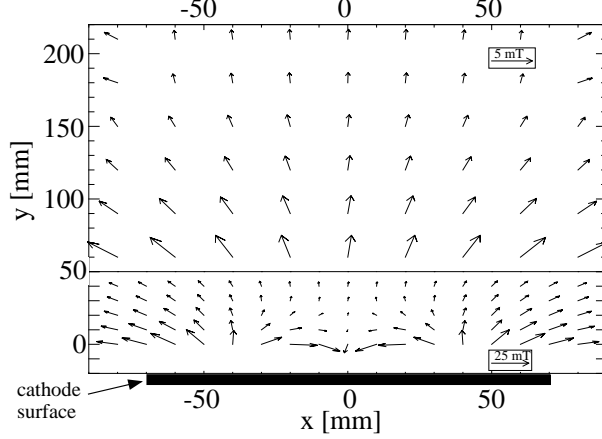
Fig. 2: Magnetic field map on the plane z = 0. The figure is split into two parts where different scales are used; the arrow length is proportional to the magnetic field strength.

of fig. 1. It consists of three tungsten wires (electrodes) having length of 3 mm, diameter of 0.2 mm and oriented parallel to the cathode; the distance between two nearby electrodes is 8 mm. Each electrode emerges from a stainless steel cylindrical pipe (diameter of 4.5 mm) and is electrically insulated from it. A 25-mm diameter stainless steel cylinder supports all three pipes and is mounted on the shaft of a manipulator allowing translation and rotation of the whole system.

In analysing Langmuir probe data it should be taken into account that: the magnetic field affects the electron current [3], the electron distribution function might not be maxwellian [4] and

the ion current does not saturate [5]. The approach is described in ref. [6]: the analysis is limited to the data up to a few volts over the floating potential; a superposition of two maxwellian electron populations is assumed (dubbed 'cold' and 'hot' electrons in the following). To model the ion current the Orbital Motion Limited theory (OML) [7] is adopted. Indeed, with the parameters used during the experiments, the mean free path turns out to be ~40 mm, much larger than 4 mm, which is the minimum value for the application of the OML theory [8] in the present conditions. Analogously to plasmas in the edge region of fusion experiments [9], a linearisation is applied to the expression of the OML ion current for maxwellian ions reported in [10]. A dimensionless voltage may be defined as $\eta = e(V_p - V)/(k_B T_c)$, where e is the elementary charge, V_p and V the plasma potential and the applied voltage, k_B the Boltzmann constant and T_c the cold electron temperature. By linearly expanding η around 30 (corresponding, for $T_c \approx 2$ eV, to 60 V, usual range for bias voltage), the total current collected by the Langmuir probe can be written as [6]:

$$I(V) = -A_{if}j_s\left[1 + R\left(V_f - V\right)\right] + A_{if}j_r\left\{\exp\left[\frac{e\left(V - V_p\right)}{k_B T_c}\right] + \frac{n_h}{n_c}\sqrt{\frac{T_h}{T_c}}\exp\left[\frac{e\left(V - V_p\right)}{k_B T_h}\right]\right\}$$

where V_f is the floating potential, $j_s = (1/2)en_\infty(k_B T_c/m_i)^{1/2}$ the ion current at V_f, $j_r = en_c[k_B T_c/(2\pi m_e)]^{1/2}$ the random cold electron current, n_∞, n_c and n_h the total, cold electron and hot electron densities in the unperturbed plasma, T_h the hot electron temperature, m_e and m_i the electron and ion masses, $A_{if} \approx 3A_{geom}$, A_{geom} the geometrical area of the cylindrical probe and $R \approx 14$ kV^{-1} if $T_c = 2$ eV.

The analysis algorithm is outlined here [6]: a linear fitting is applied to the data at negative applied voltages ($V_f - V > 40$ V); after subtracting the resulting ion current, a sum of two exponential curves is fitted to the data and the electron parameters are derived. When two slopes cannot be identified in the semilogarithmic graph of the electron current, a single-temperature analysis is performed.
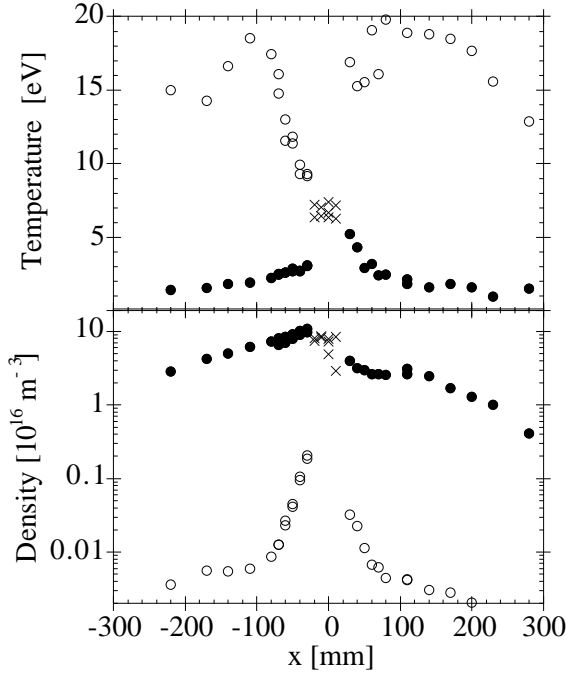
Fig. 3: Profile of electron temperature (top) and density (bottom): open and solid circles refer to hot and cold electrons respectively; crosses to the zone where one electron population is found.

Before discussing the data analysis, the discharge disturbance induced by the insertion of the probe system should be assessed. The effect on the magnetron voltage is comparable to the variation usually observed during target lifetime. A larger effect is observed in the measurements at $x > 0$ (fig. 3): in this case, the whole probe assembly was lying between the cathodes.

No appreciable difference is found between the measurements performed with different probes, giving evidence of the plasma uniformity over the probe distance in the z direction. Therefore no probe distinction will be made in the following.

In fig. 3 the profiles of electron temperature and density are shown for $y = 230$ mm and $z = 0$ at 800 W. Towards the centre ($|x| < 20$ mm) the temperatures of cold and hot electrons converge to ~7 eV. The probe I-V

characteristics show a gradual change between an outer region where a superthermal tail is detected and an inner region where the distribution function seems to be closer to a Maxwellian one. In the outer region, the hot electron density increases very steeply (characteristic length ~15 mm) by two orders of magnitude; the cold electron density increases approximately exponentially (characteristic length ~150 mm); the ratio of hot and cold electron densities ranges from ~1000 to ~10. Where a single electron population is identified, the electron density is lower than in nearby regions.
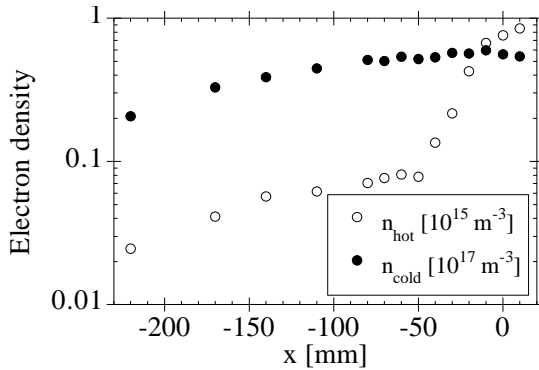
Fig. 4: Electron densities measured at y = 230 mm, z = -90 mm, 800 W.

Fig. 5: Plasma potential measured at y = 230 mm, z = 0, 800 W.

As fig. 4 shows, two electron populations are observed at any position along x for $z = -90$ mm. At this location the strong increase of the hot electron component is less pronounced (a factor of ~10) and takes place over a smaller distance (~40 mm) than at $z = 0$. Another density scan (not reported), at 800 W, $z = 0$ and $y = 330$ mm (half-way between the centre and each source), confirms that on the $z = 0$ plane a central region with one electron

component can be identified; in this case, the density gradients are steeper and the width is smaller (consistent with the magnetic map).

The floating potential decreases monotonically towards the magnetic axis. The plasma potential displays a maximum in the centre (fig. 5); an electric field of about 200 V/m can be estimated between –100 mm and 0 mm, yielding, with B≈4 mT, an $\mathbf{E}\times\mathbf{B}$ drift velocity of ~50 km/s directed along z; such a drift velocity exhibits a gradient of ~10^6 s^{-1}. In the case of one electron temperature, the plasma potential is computed by assuming the following dependence on floating potential and electron temperature: $V_p = V_f + \alpha T_e$, with $\alpha = 6$ V/eV; in the case of two electron temperatures, the plasma potential is a result of the fitting procedure.

It may be argued that in the region $|x| < 20$ mm or $|z| < 90$ mm electrons are confined, bouncing back and forth between the two sources (like in the magnetic trap [11]). Outside the central region, a layer about 40 mm thick is found, characterised by large gradients of density, plasma potential and electric field. It is possible that confinement is accomplished by this layer, though for a conclusive statement the transport across B should be measured.
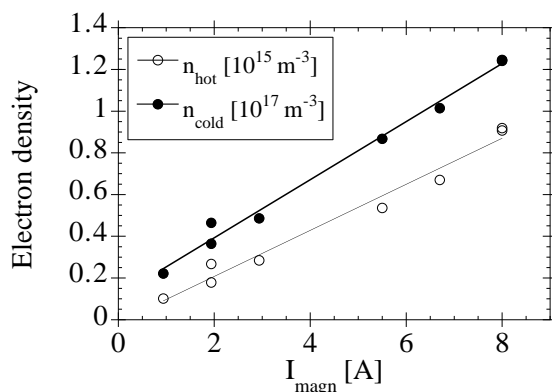
Fig. 6: Electron densities vs total current; measurements at y = 230 mm, z = -60 mm.

Plasma potential, floating potential and electron temperatures are not noticeably affected by variations of the discharge current. A fluid model [12] confirms the weak dependence of the electron temperature on the magnetron voltage. Since the discharge current is a strong function of the magnetron voltage [2] and the current density is proportional to the discharge current [1], a linear relationship can be deduced between the electron density and the magnetron current, as experimentally found (fig. 6) both for hot and cold electron densities.

To summarise, a DC magnetron sputtering device has been characterised by means of Hall and Langmuir probes. The magnetic field mapping provides the identification of the magnetic trap close to the cathode surfaces. Both magnetic and electric measurements show the existence of a central region where a single electron population is detected. Outside this region, large gradients of density, temperature, plasma potential and electric field are found. It is observed that the electron densities depend linearly on the discharge current.

[1] M. A. Lieberman, A. J. Lichtenberg, *Principles of Plasma Discharges and Material Processing*, New York, J. Wiley and Sons, 1994.
[2] A. S. Penfold, in *Handbook of Thin Film Process Technology*, IOP (1995), sec. A.3.2, p. 1.
[3] P. C. Stangeby, in *Plasma Diagnostics* (O. Auciello, D. L. Flamm Eds.), Academic Press, Boston (1988), vol. 2, p. 157; M. Tichý *et al.*, J. de Physique IV, **C4** (1997) 397.
[4] T. E. Sheridan *et al.*, J. Vac. Sci. Technol. **A 9** (1991) 688; **A 16** (1998) 2173.
[5] J. B. Friedmann *et al.*, J. Vac. Sci. Technol. **A 11** (1993) 1145.
[6] M. Spolaore *et al.*, Surface and Coatings Technology **116-119** (1999) 1022; G. Serianni *et al.*, Proc. of *XXIV Int. Conf. on Phenomena in Ionis. Gases*, Polish Academy of Sciences, Warsaw, Poland (1999), vol. II, p. 9.
[7] H. M. Mott-Smith, I. Langmuir, Phys. Rev. **28** (1926) 727.
[8] J. E. Allen, Plasma Sources Sci. Technol. **4** (1995) 234.
[9] J. P. Gunn *et al.*, Rev. Sci. Instrum. **66** (1995) 154; D. Desideri, G. Serianni, Rev. Sci. Instrum. **69** (1998) 2354.
[10] F. F. Chen, in *Plasma Diagnostic Techniques* (R. H. Huddlestone, S. L. Leonard Eds.), Academic Press, New York (1965), p. 113.
[11] T. E. Sheridan *et al.*, J. Vac. Sci. Technol. A **16** (1998) 2173.
[12] J. W. Bradley, Plasma Sources Sci. Technol. **7** (1998) 572.